HOSTED BY

ELSEVIER

Original article

Targeting XGHPRT enzyme to manage *Helicobacter pylori* induced gastric cancer: A multi-pronged machine learning, artificial intelligence and biophysics-based study

Alhumaidi B. Alabbas

Department of Pharmaceutical Chemistry, College of Pharmacy, Prince Sattam Bin Abdulaziz University, Al Kharj, Saudi Arabia

A B S T R A C T

Helicobacter pylori infects the stomach mucosa of over half of the global population and can lead to gastric cancer. This pathogen has demonstrated resistance to many frequently prescribed antibiotics, thereby underscoring the pressing need to identify novel therapeutic targets. The inhibition or disruption of nucleic acid biosynthesis constitutes a promising avenue for either restraining or eradicating bacterial proliferation. The synthesis of RNA and DNA precursors (6-oxopurine nucleoside monophosphates) is catalyzed by the XGHPRT enzyme. In this study, using machine learning, artificial intelligence and biophysics-based software, CHEMBRIDGE-10000196, CHEMBRIDGE-10000295, and CHEMBRIDGE-10000955 were predicted as promising binders to the XGHPRT with a binding score of −14.20, −13.64, and −12.08 kcal/mol, respectively, compared to a control guanosine-5′-monophosphate exhibiting a docking score of −10.52 kcal/mol. These agents formed strong interactions with Met33, Arg34, Ala57, Asp92, Ser93, and Gly94 at short distance. The docked complexes of the lead compounds exhibited stable dynamics during the simulation time with no global changes noticed. The docked complexes demonstrate a significantly stable MM-GBSA and MM-PBSA net binding energy of −60.1 and −61.18 kcal/mol for the CHEMBRIDGE-10000196 complex. The MM-GBSA net energy value of the CHEMBRIDGE-10000295 complex and the CHEMBRIDGE-10000955 complex is −71.17 and −65.29 kcal/mol, respectively. The CHEMBRIDGE-10000295 and CHEMBRIDGE-10000955 complexes displayed a net value of −71.91 and −63.49 kcal/mol, respectively, as per the MM-PBSA. The major driving intermolecular interactions for the docked complexes were found to be the electrostatic and van der Waals. The three filtered molecules hold potential for experimental evaluation of their potency against the XGHPRT enzyme.

1. Introduction

The presence of *Helicobacter pylori* (*H. pylori*) in the stomach mucosa has been linked to the development of peptic ulcers, gastritis, gastric adenocarcinoma, and lymphoid tissue lymphoma. In 1982, the causal relationship between *H. pylori* and various gastric illnesses was discovered, thanks to the research conducted by Warren and Marshall. Their groundbreaking work was later recognized with a Nobel Prize in Physiology and Medicine in 2005 (Australia and Robin, 2005). The bacterium is identified in about 50 % of the human population and up to 100 % in some regions (Mezmale et al., 2020). The bacteria infection is often asymptomatic but causes serious symptoms of peptic ulcers and gastritis (Kim and Wang, 2021; Liou et al., 2020). *H. pylori* is ranked third after hepatitis B and papillomavirus as the causative agent of cancer (Coates et al., 2020).

The emergence of novel antibiotic resistance mechanisms in Gram-negative bacterial infections is a significant concern in the healthcare industry. The prevalence of multi-drug resistant (MDR), extensive drug-resistant (XDR), and pan-drug resistant (PDR) strains is on the rise, which poses a significant threat to the efficacy of antibiotics. The development of effective leads to combat this rise in antibiotic resistance is of paramount importance to ensure the safety and well-being of patients (Hutchings et al., 2019). The drug resistance is up to 15–20 % and even higher. The pathogen is listed WHO list of 12 bacterial pathogens that need prompt action to highlight new drug targets and identify antibiotics (Tacconelli et al., 2018a, 2018b). Among the several biological targets that can be targeted for treating *H. pylori* infections, nucleic acid metabolic production could be an innovative target (Keough et al., 2021). Interrupting nucleic acid biosynthesis can significantly diminish the pathogen's ability to grow and survive. *H. pylori* transports purine

bases from the host, which is compulsory as this process is vital to the synthesis of DNA/RNA (Sangavai et al., 2020). Previously, a study has established that xanthine-guanine-hypoxanthine phosphoribosyltransferase (XGHPRT) is a key enzyme for the constant production of purine nucleotide monophosphates (Keough et al., 2021). Considering this, the XGHPRT is a vital target for drug intervention.

The XGHPRT has been documented previously as an attractive target against *Plasmodium vivax, Mycobacterium tuberculosis,* and *Plasmodium falciparum* (Hedstrom, 2009; Keough et al., 2018, 2015). Nucleoside phosphonate inhibitors have been designed to mimic substrates of enzyme catalysis (Keough et al., 2009). Considering the chemotherapeutic importance of XGHPRT, herein, in this study several bioinformatic approaches and software using machine learning, artificial intelligence and biophysics-based principles are utilized to identify strong binding small molecules to the enzyme active pocket. The traditional process of drug discovery is resource-intensive and a lengthy task. As such, the integration of information technology with chemistry proved successful in streamlining drug design, discovery, and optimization (Macalino et al., 2015; Sydow et al., 2019; Talele et al., 2010). Additionally, it assists in hit-to-lead selection and facilitates profiling of compounds' absorption, distribution, metabolism, excretion, and toxicity (ADMET). The recognition of small molecules in this study presents a promising avenue for the control of *H. pylori* infections, pending experimental validation in animal models. The potential implications of this finding are significant, as effective treatments for H. pylori infections are currently limited. Further research is warranted to better understand the mechanism of action of these molecules, as well as their efficacy and safety profiles. If validated, these molecules could represent a welcome addition to the arsenal of H. pylori treatments currently available and could have meaningful implications on public health.

2. Materials and methods

2.1. ChemBridge drug library preparation

Selected compounds from the ChemBridge database were used in virtual screening against *H. pylori* XGHPRT. In total of 3928 molecules were used in the library. ChemBridge is a library of high-quality screening compounds for hits identification. The library for the last three decades provided a source of novel drug-like molecules to fulfill the requirements of modern drug discovery in both academia and industry. The ChemBridge currently holds more than 1.3 million compounds that are available for biological activity testing. The selected molecules are Food and Drug Administration (FDA) approved drugs. The imported library went through energy minimization using the MM2 force field within the PyRx 0.8 software. Following this, the compounds were transformed into.pdbqt format (Dallakyan and Olson, 2015; Halgren, 1996).

2.2. Receptor enzyme structure preparation

The crystal structure of the *H. pylori* XGHPRT enzyme was imported from the protein database (PDB) in UCSF Chimera v1.16 (Kaliappan and Bombay, 2018) by entering the PDB code of 7KL7 (Keough et al., 2021). The entry is very recent and made available on 05/05/2021 and has a resolution value of 1.47 Å. The crystal structure weighs 37.41 kDa and has an atom count of 2,731. The PDB database is handled by Brookhaven National Laboratory with more than 8,000 entries (Sussman et al., 1998). The database has housed the crystal structure of nucleic acids, proteins, enzymes, and other biological macromolecules. The retrieved structure was preprocessed in UCSF Chimera, where all co-crystallized ligands and water molecules were eliminated. Next, the energy of the structure was minimized using conjugate gradient and steepest descent algorithms for 2,000 iterations. The energy minimization procedure is vital to discard any steric clashes present in the structure and add

missing atoms. The energy-minimized structure, in an analysis conducted by PDBSum, revealed that 91 % of the enzyme lies in the most favored regions of the Ramachandran plot and zero residues in the disallowed regions (Laskowski et al., 2018). This illustrated the good quality of the energy-minimized enzyme structure.

2.3. Prediction of active site

The active site of the XGHPRT enzyme was evaluated using the PrankWeb server (Jendele et al., 2019) available at (https://prankweb.cz/). The PrankWeb server is an online platform to give predictions about active sites.

2.4. PyRx virtual screening

To carry out the structure-based virtual screening (SBVS) of the drug library, the AutoDock Vina v4.2.6 platform available in PyRx 0.8 was used (Dallakyan and Olson, 2015). In the PyRx, the molecules and receptor enzyme were converted into.pdbqt, and then a docking protocol was conducted. The dimensions of the grid box were configured along the X-axis (24.14 Å), Y-axis (−1.88 Å), and Z-axis (86.80 Å). The dimensions of the box were defined as 25 Å for each of the three coordinates, X, Y, and Z. The number of conformers for each compound generated was 100. In the process of evaluating compounds for their potential to bind to the XGHPRT enzyme, the best-docked conformation is determined according to its lowest binding energy in units of kcal/mol. Subsequently, Discovery Studio Visualizer v2021 and UCSF Chimera v1.16 were employed to visualize the best-docked complexes (Biovia, 2017; Kaliappan and Bombay, 2018).

2.5. AMBER molecular dynamics simulation

The molecular dynamic simulation (MDS) study of selected top complexes was accomplished by AMBER v22 software (Case et al., 2005). The antechamber program was utilized to produce the parameter files for the docked complexes (Wang et al., 2001). The compounds' partial charge, bond angle, and length parameterization were done using the AMBER General Force Field (GAFF) and the receptor enzyme parameters were generated using FF14Sb (Maier et al., 2015; Sprenger et al., 2015). The complexes were positioned within a TIP3 water box with a padding distance of 12 Å. The CHEMBRIDGE-10000196 complex, CHEMBRIDGE-10000295 complex, CHEMBRIDGE-10000955 complex, and control system had 15, 13, 18, and 10 counter ions added, respectively. The process of energy minimization for the docked structure was executed using two widely accepted methods, namely the steepest descent and conjugate gradient methods. The first algorithm was applied for 1,500 rounds, while the latter one was used for 2,000 steps to get complete energy-minimized systems. An ensemble equilibration of the studied complexes was carried out using the number of particles, volume, and temperature (NVT) ensemble for 500 ps. This was followed by conducting the NVT ensemble using the Berendsen barostate for 1 ns while keeping the pressure at 1 bar. During the production run, the temperature was conserved using the Langevin algorithm for a duration of 200 ns. (Izaguirre et al., 2001). The SHAKE algorithm was applied to preserve bonds containing hydrogen atoms during the MDS (Andersen, 1983). The Particle Mesh Ewald Method was implemented to manage the long-range electrostatic interactions. The simulation trajectories were examined utilizing the CPPTRAJ module, and for plotting purposes, XMGRACE v5.1 software was used (Roe and Cheatham, 2013; Turner, 2005).

2.6. MM-PBSA binding free energy analysis and revalidation

The calculation of the binding free energies of complexes was conducted using the AMBER MMPBSA.py module, based on the Molecular Mechanics-Poisson Boltzmann Surface Area (MM-PBSA) method (Miller
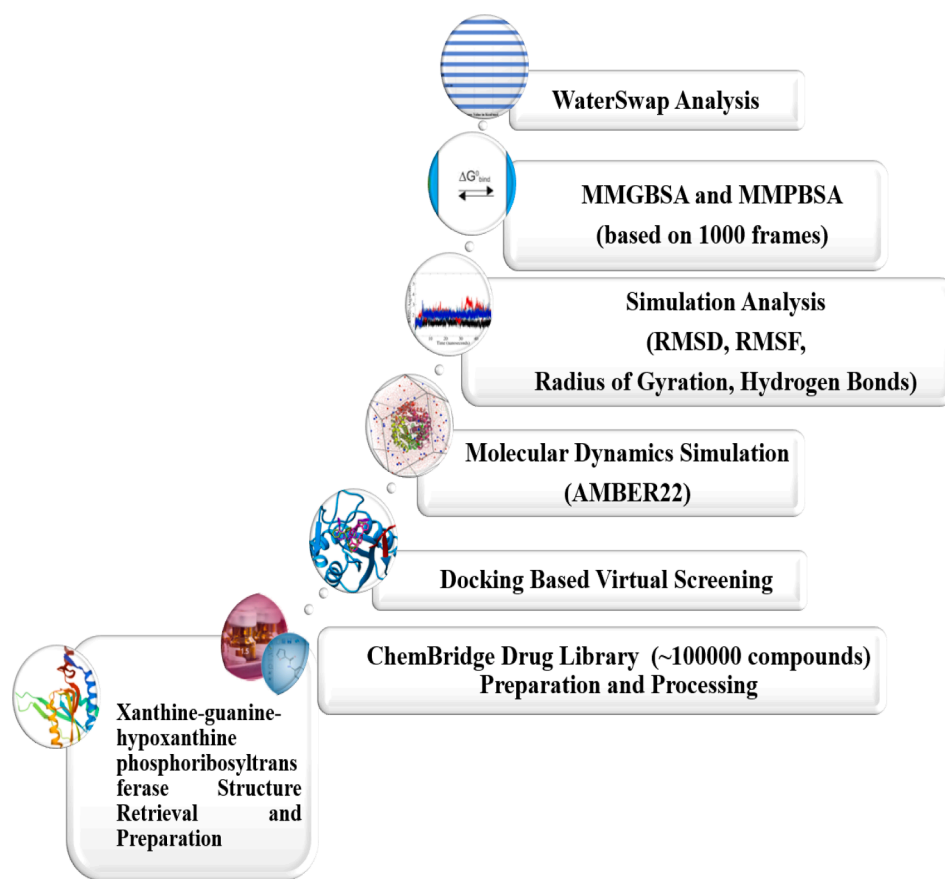
Fig. 1. The stepwise flow of different steps utilized in the current study. The study started with the retrieval of the xanthine-guanine-hypoxanthine phosphor-ibosyltransferase structure. Then it was used in different phases i.e., SBVS, MDS studies, MMGBSA and MMPBSA binding free energies analysis and WaterSwap-based absolute binding free energy prediction.

et al., 2012; Navid et al., 2021). In this experiment, a sum of 2,000 frames was considered from simulation trajectories with the same interval of 1 ns. The MM-PBSA free energies were revalidated using WaterSwap, a more advanced method for swapping equal volumes of water molecules with ligands occupying the enzyme's active site cavity (Tahir ul Qamar et al., 2021; Woods et al., 2014).

2.7. ADMET profiling

The profiling of molecules for ADMET properties was conducted utilizing ADMETlab 2.0 (available online at https://admetmesh.scbdd.com/). This online integrated platform provides meticulous prediction of ADMET properties of small molecules (Xiong et al., 2021). The ADMETlab 2.0 is considered the enhanced version of ADMETlab for evaluating medicinal and physicochemical properties as well as ADMET properties. Though other ADMET software is available, ADMETlab 2.0 provides a wide spectrum of analysis and is trained with a better dataset (Xiong et al., 2021). The comprehensive procedure of the study is depicted in Fig. 1.
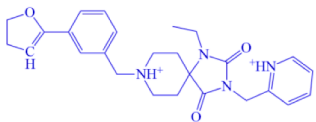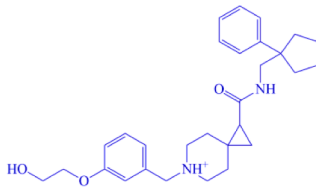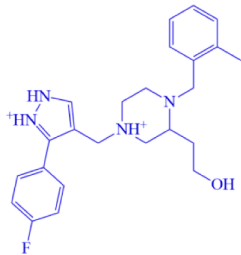
3. Results

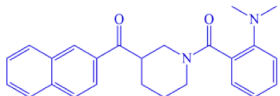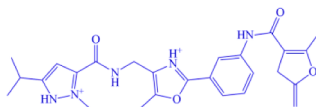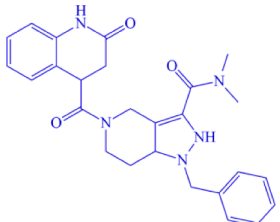*3.1. Structure-based virtual screening*

The SBVS process began by identifying the active pocket of the *H. pylori* XGHPRT enzyme using the PrankWeb server. The server predicted two pockets with scores of 22.78 and 20.41, as shown in S-Table 1. During the virtual screening process, three molecules from the ChemBridge database, namely CHEMBRIDGE-10000196, CHEM-BRIDGE-10000295, and CHEMBRIDGE-10000955, were identified as promising binders of the enzyme. These molecules had a binding energy score of −14.20, −13.64, and −12.08 kcal/mol, respectively, compared to a control guanosine-5′-monophosphate, which had a docking score of −10.52 kcal/mol. The details of the top 10 molecules, including their binding energy score, IUPAC naming, and key residues involved in interactions are summarized in Table 1.

The majority of the library compounds were seen docked at the central cavity, which is the natural binding site for substrate during enzyme catalysis (Fig. 2). CHEMBRIDGE-10000196 major contribution was noticed from the terminal 1-ethyl-2,4-dioxo-3-(pyridin-1-ium-2-ylmethyl)-1,3,8-triazaspiro[4.5]decan-8-ium moiety which produces hydrogen bonds with Gly94, Asn95 and Ser96 at a distance of 2.6 Å, 2.8 Å and 2.1 Å, respectively. In addition to the above, the analysis showed the presence of numerous van der Waals and pi-alkyl interactions. The 2-(m-tolyl)-2,5-dihydrofuran ring is mainly engaged in weak hydrophobic contacts (Fig. 3). The CHEMBRIDGE-10000295 2-(m-tolyloxy)ethanol favored to form strong interactions with Gly94, Asn95, and Ser96 with a distance of 2.9 Å, 3.1 Å and 2.5 Å, respectively. The opposite ring contributed small in overall binding with the enzyme (Fig. 3). The CHEMBRIDGE-10000955 interaction with the enzyme is primarily influenced by van der Waals contacts. The following residues were seen in weak hydrophobic contacts; Val32, Arg34, Gly35, Ala57, Ile58, Leu69, Asp88, Asp92, Ser93, Asn95, Ser96 and Leu97. Only, one hydrogen bond with the Leu97 was noticed (Fig. 3). In all the docked complexes, it was noticed that both van der Waals and hydrogen bonds were essential in keeping a stable ligand binding to the XGHPRT active site residues (Du et al., 2016).
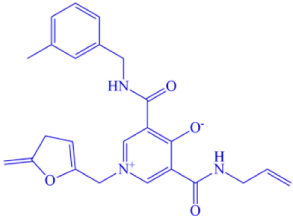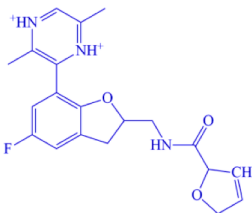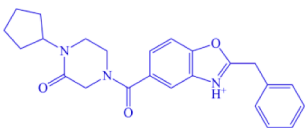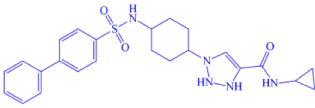
Table 1

Lead compounds identified in structure-based virtual screening. Each compound 2D structure along with IUPAC naming, binding energy score. The amino acid residues participating in the hydrogen bondings and van der Waals interactions are also given.

Rank	Compound ID	2D Structure	IUPAC Name	Binding Energy Score	H-Bonds	Van der Waals Interactions
1	CHEMBRIDGE-10000196		8-(3-(4,5-dihydrofuran-2-yl)benzyl)-1-ethyl-2,4-dioxo-3-(pyridin-1-ium-2-ylmethyl)-1,3,8-triazaspiro[4.5]decan-8-ium	−14.20	Gly94 Asn95 Ser96	Ser59, Asp88, Ile90, Val91, Ser93, Leu97, Lys12, Ile139, Phe14, Glu144
2	CHEMBRIDGE-10000295		6-(3-(2-hydroxyethoxy)benzyl)-1-(((1-phenylcyclopentyl)methyl)carbamoyl)-6-azaspiro[2.5]octan-6-ium	−13.64	Gly94 Asn95 Ser96	Val32, Arg34, Gly35, Leu69, Asp92, Ser93, Leu97, Ile139, Phe141, Glu144
3	CHEMBRIDGE-10000955		1-((3-(4-fluorophenyl)-1H-pyrazol-2-ium-4-yl)methyl)-3-(2-hydroxyethyl)-4-(2-methylbenzyl)piperazin-1-ium	−12.08	Leu97	Val32, Arg34, Gly35, Ala57, Ile58, Leu69, Asp88, Asp92, Ser93, Asn95, Ser96, Leu97
4	CHEMBRIDGE-10000111		(3-(2-naphthoyl)piperidin-1-yl)(2-(dimethylamino)phenyl)methanone	−11.33	Ser96	Arg34, Gly35, Ala57, Ser59, Asp88, Glu89, Val91, Asp92, Ser93, Leu97, Ile139, Phe141, Glu144
5	CHEMBRIDGE-10000290		4-((5-isopropyl-2-methyl-1H-pyrazol-2-ium-3-carboxamido)methyl)-5-methyl-2-(3-(2-methyl-5-methylene-4,5-dihydrofuran-3-carboxamido)phenyl)oxazol-3-ium	−10.83	Arg34 Ala57 Ser93	Val32, Met33, Gly35, Asn56, Ile58, Ser59, Leu69 Asp88, Ile90, Val91, Gly94, Ser96, Leu97
6	CHEMBRIDGE-10000550		1-benzyl-N,N-dimethyl-5-(2-oxo-1,2,3,4-tetrahydroquinoline-4-carbonyl)-2,4,5,6,7,7a-hexahydro-1H-pyrazolo[4,3-c]pyridine-3-carboxamide	−10.06	Ser93	Met33, Gly35, Asn56, Ala57, Asp88 Glu89, Ile90 Val91, Asp92, Gly94, Ser96 Leu97, Gly144

Table 1 (*continued*)

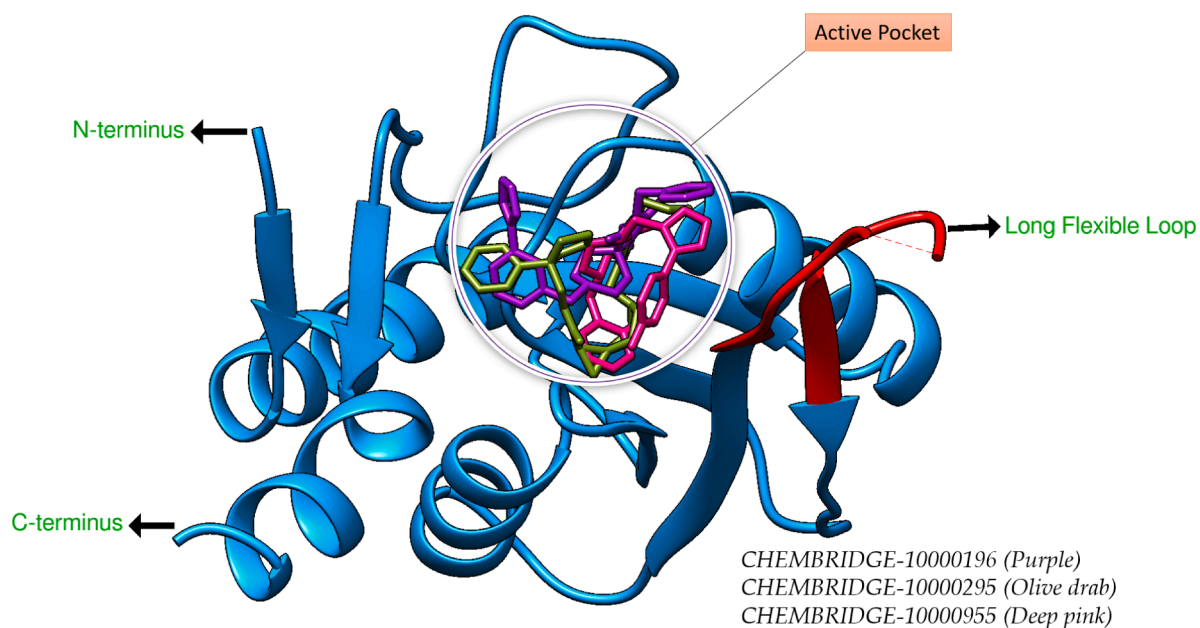| Rank	Compound ID	2D Structure	IUPAC Name	Binding Energy Score	H-Bonds	Van der Waals Interactions
7	CHEMBRIDGE-10001663		3-(allylcarbamoyl)-5-((3-methylbenzyl)carbamoyl)-1-((5-methylene-4,5-dihydrofuran-2-yl)methyl)pyridin-1-ium-4-olate	−9.67	Asp88 Ser96	Val32, Gly35, Ala57, Ser59 Leu69, Gly89, Ile90, Val91, Asp92, Asn95, Leu97, Ile139, Phe141, Gly144
8	CHEMBRIDGE-10001746		3-(2-((2,5-dihydrofuran-2-carboxamido)methyl)-5-fluoro-2,3-dihydrobenzofuran-7-yl)-2,5-dimethylpyrazine-1,4-diium	−8.31	Arg34 Ile90 Ser93	Val32, Gly35, Ser39, Ala57, Ile58, Asp88, Val91, Gly94, Asp92, Asn95, Ser96, Leu97
9	CHEMBRIDGE-10001776		2-benzyl-5-(4-cyclopentyl-3-oxopiperazine-1-carbonyl)benzo[d]oxazol-3-ium	−8.04	Met33 Arg34 Ala57 Asp92 Gly94	Gly35, Ser59, Asp88, Glu89, Ile90, Val91, Ser93, Asn95, Ser96, Leu97
10	CHEMBRIDGE-10001792		1-(4-([1,1′-biphenyl]-4-ylsulfonamido)cyclohexyl)-N-cyclopropyl-2,3-dihydro-1H-1,2,3-triazole-4-carboxamide	−8.07	Gly35 Asp88 Gly89 Ile90	Val32, Arg34, Gly36, Ala57, Ser59, Thr62, Asp92, Gly94

Fig. 2. The three-dimensional conformation of docked compounds at *H. pylori* xanthine-guanine-hypoxanthine phosphoribosyltransferase active pocket. The XGHPRT's N-terminus, C-terminus, and long flexible loop are highlighted.
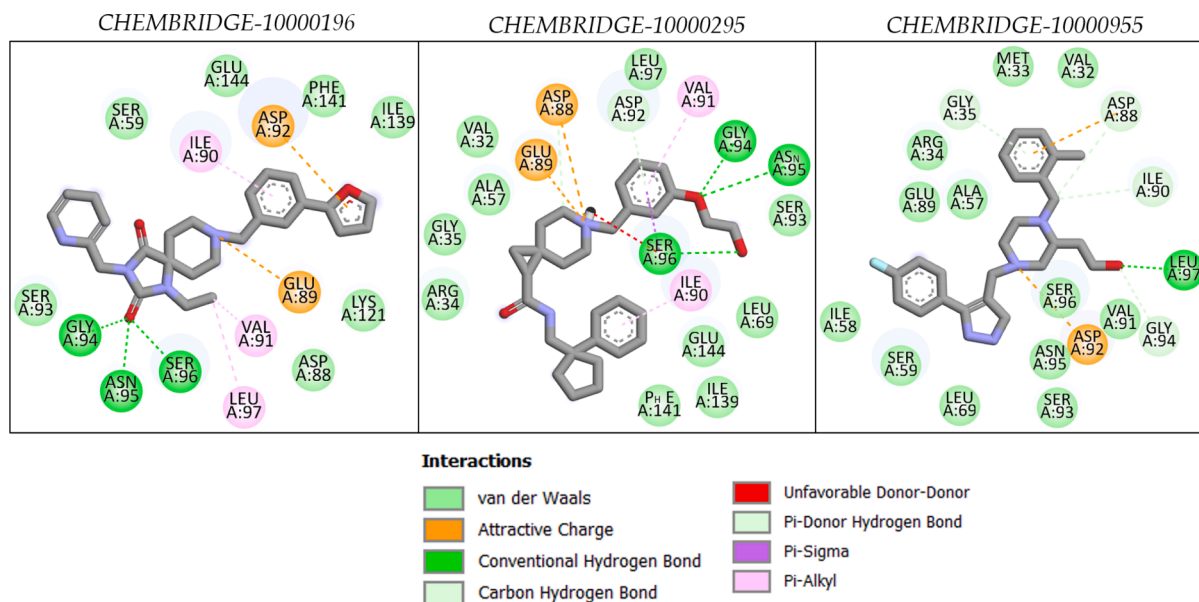
Fig. 3. The chemical interactions plotting of compounds with the *H. pylori* xanthine-guanine-hypoxanthine phosphoribosyltransferase active pocket residues.

3.2. Understanding docked systems' movements

Even though molecular docking studies are highly useful in terms of the prediction of intermolecular docking conformation and predicting the binding energy of docked ligand(s), nevertheless, they only provide information on a single static binding mode (Ahmad et al., 2019a; El Bakri et al., 2021; Shaker et al., 2021). As the apo biomolecules and docked biomolecules behave in dynamics, understanding complex movements as a function of time is vital to guiding atomic-level interactions between the receptor residues and ligands. The simulation trajectories were resolved using Newton's equation of motion and plots were generated to decipher the complexes' stability and deviation along the simulation time. The evaluation of the root mean square deviation (RMSD) was conducted by taking into consideration the carbon alpha atoms. RMSD is a key parameter to highlight whether the system under investigation is in an equilibrium state or not (Maiorov and Crippen, 1994). The backbone structure conformation of complexes is plotted versus time. The RMSD analysis of all complexes is provided in Fig. 4A. Notably, all the studied complexes were observed in stable conformation with very minor variations observed throughout the time. The mean RMSD of the CHEMBRIDGE-10000196 complex, CHEMBRIDGE-10000295 complex, CHEMBRIDGE-10000955 complex, and control system is 1.68 Å, 1.42 Å, 1.76 Å and 1.77 Å, respectively. It is very noticeable that the studied systems showed stable dynamics compared to control systems. This is again a confirmation of strong intermolecular affinity and stable binding mode throughout simulation time. Secondly, as the interactions between the compounds and receptors are guided by the binding site residues, it is important to examine the residue level stability and fluctuations (Ahmad et al., 2017). The minor structure deviations were noticed due to loops of the receptor enzyme that upon compounds binding showed flexibility. This was achieved by evaluating the root mean square fluctuation (RMSF), which was done on backbone carbon alpha atoms (Fig. 4B). A coherence in the findings was noticed. The mean RMSF of the CHEMBRIDGE-10000196 complex, CHEMBRIDGE-10000295 complex, CHEMBRIDGE-10000955 complex, and control system is 1.43 Å, 1.23 Å, 1.18 Å and 1.87 Å, respectively. The bulk of the active site residues: Met33, Arg34, Ala57, Asp92, Ser93, and Gly94 were found to have very stable RMSF values (<2 Å). The small fluctuating regions were those present in the loops, which are naturally flexible and the deviations may contribute to ligand adjustment during enzyme natural catalysis. Further, surety about the

complexes' stable nature and equilibrium and compact behavior was derived from the radius of gyration (Rg) analysis (Lobanov et al., 2008). According to this analysis, the complexes displayed a strong docked behavior (Fig. 4C). The Rg values for the CHEMBRIDGE-10000196, CHEMBRIDGE-10000295, and CHEMBRIDGE-10000955 complexes along with the control system were measured and compared. The average Rg values were found to be 56.32 Å, 53.87 Å, 55.69 Å, and 57.02 Å, respectively.

3.3. Estimation of binding free energies

The nature of compounds binding to xanthine-guanine-hypoxanthine phosphoribosyltransferase in terms of chemical interactions was investigated through simulation trajectories based on endpoint binding free energy methods like MM-PBSA and molecular mechanics generalized Born surface area (MM-GBSA) (Alamri et al., 2022; Fatima et al., 2022; Miller et al., 2012; Wang et al., 2019). Both these methods are appreciable in terms of speed and accuracy. According to the data shown in Table 2, it is apparent that all the docked complexes have demonstrated a notably stable net binding energy. The CHEMBRIDGE-10000196 complex demonstrated MM-GBSA and MM-PBSA values of −60.1 and −61.18 kcal/mol, respectively. The MM-GBSA net energy values of CHEMBRIDGE-10000295 complex and CHEMBRIDGE-10000955 complex were −71.17 and −65.29 kcal/mol, respectively, whereas the MM-PBSA net values reported for the same complexes were −71.91 and −63.49 kcal/mol, respectively. The values indicate the system's high intermolecular affinity and docked conformation stability, resulting in very stable energies throughout the simulation period. The gas phase energy was determined as the major driving energy for stabilizing the intermolecular interactions, especially the van der Waals force, which dictates the energy parameters. The van der Waals energy values for the CHEMBRIDGE-10000196 complex, CHEMBRIDGE-10000295 complex and CHEMBRIDGE-10000955 complex were −56.89, −64.82, and −58.92 kcal/mol, respectively. The dominance of van der Waals contacts was evident from the molecular docking section, where the compounds were noticed along the length to produce short, intermediate, and long-distance van der Waals bonding. Another force of the gas phase energy that contributed to the global stability of complexes was electrostatic energy. The net electrostatic energy values of the CHEMBRIDGE-10000196 complex, CHEMBRIDGE-10000295 complex, and CHEMBRIDGE-10000955 complex were
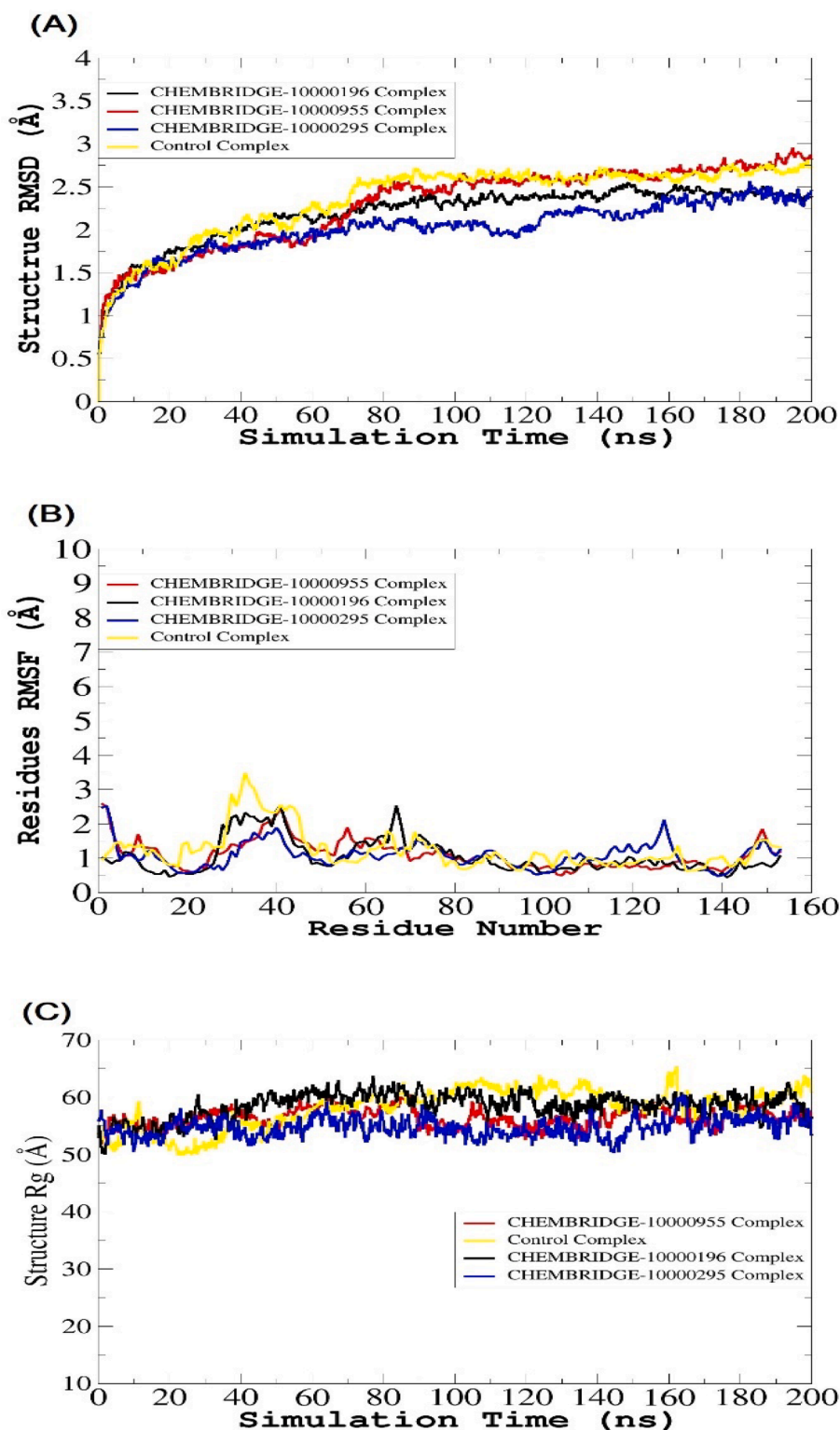
Fig. 4. The time-dependent dynamics of docked complexes and their behavior over a duration of 200 ns. The analysis comprised three key parameters, namely (A) RMSD, (B) RMSF, and (C) Rg, with a specific focus on the carbon alpha atoms of the complexes.

−22.63, −24.06, and −25 kcal/mol, respectively. This is another confirmation that both electrostatic and van der Waals energies balance the recognition and docking of compounds to the active pocket of xanthine-guanine-hypoxanthine phosphoribosyltransferase. According to the net energy value calculated using both MM-PBSA and MM-GBSA, the complex of CHEMBRIDGE-10000295 was ranked as the most stable complex in comparison to the other two systems. The solvation energy

was predicted to be non-favorable due to the negative contribution to complex formation. The net MM-GBSA solvation energy for complexes was in the following order; CHEMBRIDGE-10000196 complex (19.42 kcal/mol), CHEMBRIDGE-10000295 complex (17.71 kcal/mol), and CHEMBRIDGE-10000955 complex (18.63 kcal/mol). The solvation energy values for the CHEMBRIDGE-10000196 complex, CHEMBRIDGE-10000295 complex and CHEMBRIDGE-10000955 complex were
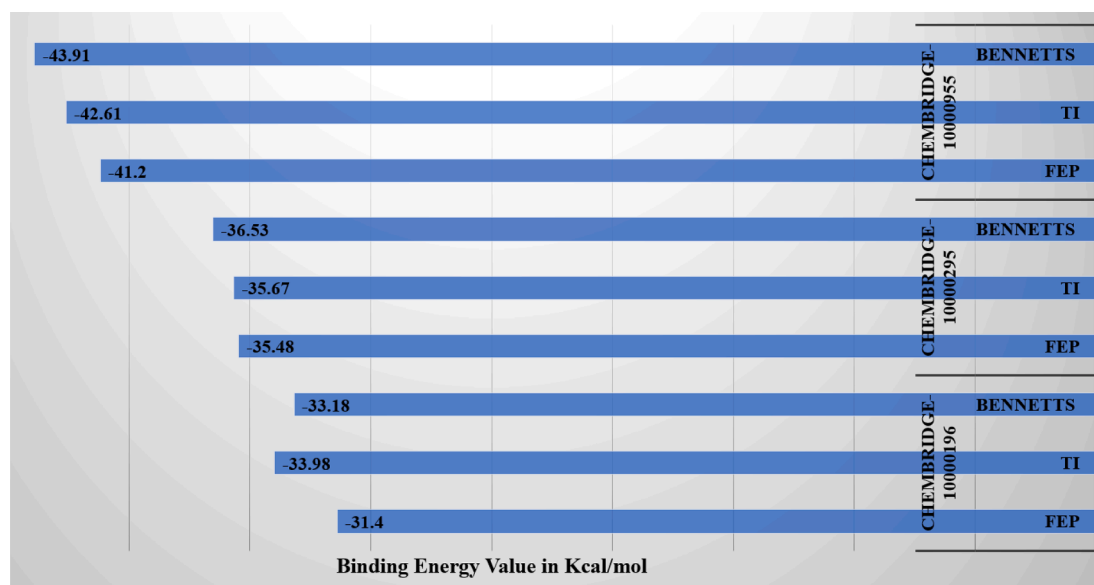
Table 2

Free energy values estimated by MM-GBSA and MM-PBSA methods. All the values are expressed in kcal/mol.

Method	Energy Parameter	CHEMBRIDGE-10000196	CHEMBRIDGE-10000295	CHEMBRIDGE-10000955	Control Complex
MM-GBSA	Van der Waals Energy	−56.89	−64.82	−58.92	−44.10
	Electrostatic Energy	−22.63	−24.06	−25.00	−16.50
	Delta Gas Phase Energy	−79.52	−88.88	−83.92	−60.6
	Delta Solvation Energy	19.42	17.71	18.63	11.84
	Net Energy	−60.1	−71.17	−65.29	−48.76
MM-PBSA	Van der Waals Energy	−56.89	−64.82	−58.92	−44.10
	Electrostatic Energy	−22.63	−24.06	−25.00	−16.50
	Delta Gas Phase Energy	−79.52	−88.88	−83.92	−60.6
	Delta Solvation Energy	18.34	16.97	20.43	10.83
	Net Energy	−61.18	−71.91	−63.49	−49.77

Table 3

AMBER normal mode entropy estimation for complexes. The values are in kcal/mol.

Complex	Translational	Rotational	Vibrational	Total	DELTA S total
CHEMBRIDGE-10000196	18.28 (0.15)	21.33 (0.20)	2515.03 (1.64)	2,554.64	−2.41
CHEMBRIDGE-10000295	24.11 (0.52)	22.16 (0.43)	2634.05 (2.49)	2,680.32	3.85
CHEMBRIDGE-10000955	20.64 (0.81)	21.86 (0.71)	2420.78 (4.19)	2,463.28	5.20
Control	18.34 (0.52)	14.12 (0.55)	2228.10 (3.34)	2,260.56	11.62

Fig. 5. The binding free energies calculated by different algorithms of WaterSwap including free energy perturbation (FEP), thermodynamic integration (TI) and Bennetts algorithm. The resultant values are presented in units of kcal/mol.

18.34, 16.97, and 20.43 kcal/mol, respectively. Compared to the lead systems, the control complex secured less binding energy scores. The net MM-GBSA control complex energy value was −48.76 kcal/mol, while the MM-PBSA net energy value was −49.77 kcal/mol. Details of the control system and the lead complexes energies are tabulated in Table 2.

3.4. Prediction of entropy energy

Further confirmation of the intermolecular docked complexes was accomplished using AMBER normal mode entropy energy estimation (Ahmad et al., 2018). The entropy energy estimation is very costly, so limited simulation frames were analyzed in the AMBER normal mode entropy calculation (Genheden et al., 2012). The entropy energy of systems was split into translational, rotational, and vibrational energy. The CHEMBRIDGE-10000196 complex was depicted as the most stable in terms of having less disorder energy. The net energy value of the CHEMBRIDGE-10000196 complex was −2.41 kcal/mol. The CHEMBRIDGE-10000295 complex and CHEMBRIDGE-10000955 complex were found to have unstable entropy energy scores of 3.85 kcal/mol

and 5.20 kcal/mol, respectively. The control system was ranked unstable compared to other complexes. The AMBER normal entropy energy score for each complex is given in Table 3.

3.5. WaterSwap analysis

The MM-GBSA and MM-PBSA methods for binding free energy predictions though quite popular, still suffer from some drawbacks. For example, the influence of water molecules that connect the ligand with receptor residue atoms is not factored in during calculation. On the other hand, the WaterSwap considers the ligand-water and receptor-water interactions. This method has been implicated in many studies in recent times to validate the docking and MM-PBSA findings (Ahmad et al., 2019b; Raza et al., 2019). The WaterSwap analysis utilizes three distinct algorithms to execute free energy calculations, namely free energy perturbation (FEP), thermodynamic integration (TI), and the Bennetts algorithm (Bergström and Larsson, 2018; Woods et al., 2014). CHEMBRIDGE-10000955 was determined as the most stable with energy values of −43.91 (kcal/mol; Bennetts), −42.61 (kcal/mol; TI), and
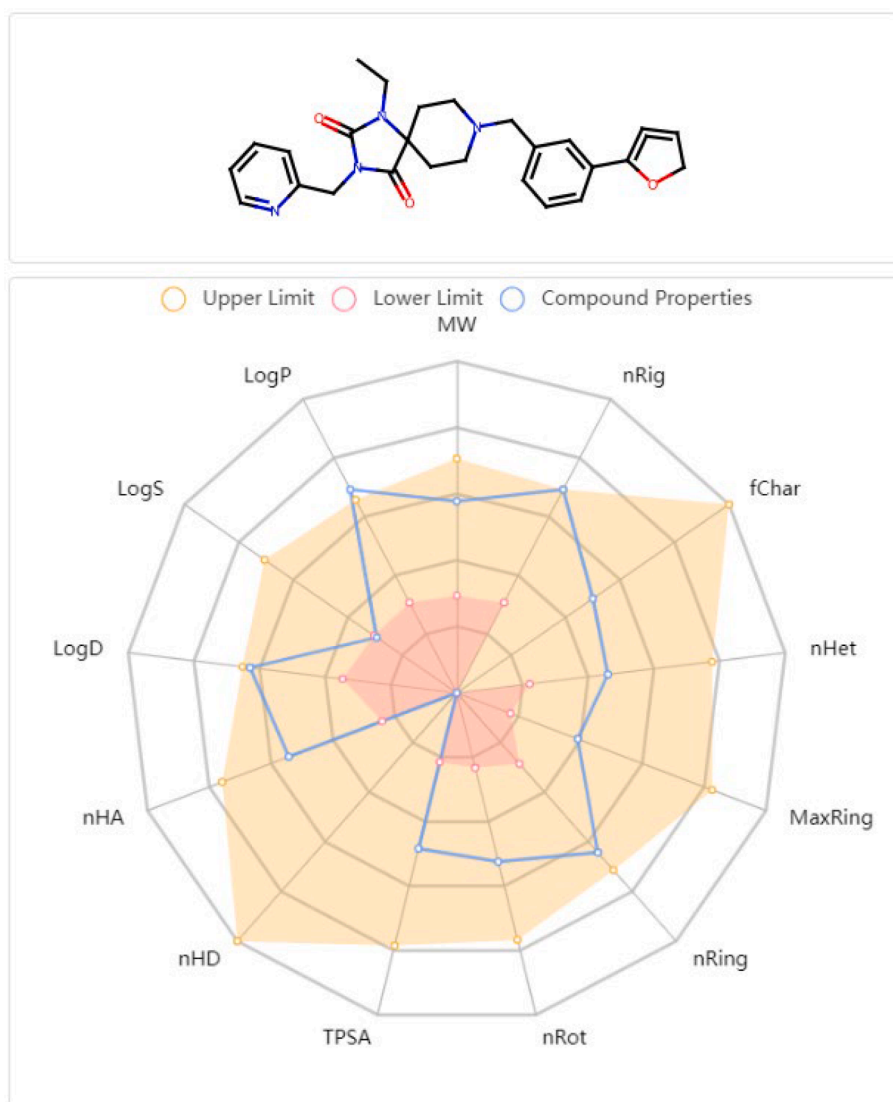
Fig. 6. ADMET profiling of CHEMBRIDGE-10000196. The yellow shadow and pink regions represent upper limits and lower limits, respectively while the blue line stands for compound properties. (For interpretation of the references to colour in this figure legend, the reader is referred to the web version of this article.)

−41.2 (kcal/mol; FEP). The algorithms have scored < 1 kcal/mol, indicating well-converged systems (Fig. 5). The very negative scoring in WaterSwap demonstrates the complexes showed tremendous stable dynamics with strong intermolecular conformation and interactions.

3.6. ADMET profiling of lead molecules

The bad and undesirable ADMET properties of lead molecules collected after a tedious drug discovery process may result in late-stage attrition (Pires et al., 2015). Thus, ADMET profiling of compounds at early stages can bring new dimensions to potent drug development (Alamri et al., 2023; Altharawi et al., 2021; Jia et al., 2019). The computational methods in ADMET profiling provide faster prediction and are economically viable with no need for expensive laboratory resources. The CHEMBRIDGE-10000196, CHEMBRIDGE-10000295, and CHEMBRIDGE-10000955 compounds' properties against upper and lower limits are plotted as radar and given in Figs. 6, 7, and 8, respectively. The properties of the compound that have been analyzed include its molecular weight (MW), the number of rings (nRig), the number of heteroatoms (nhet), formal charge (fchar), the number of atoms in the biggest ring (MaxRing), the number of rotatable bonds (nRot), the number of rigid bonds (nRig), the number of hydrogen bond donors

(nHD), the number of hydrogen bond acceptor (nHA) and the topological polar surface area (TPSA). All three lead molecules identified herein were found to satisfy the physicochemical properties limits of the ADMETlab 2.0 radar; thus, they can be classified as good drug molecules and possess properties that can make them good lead molecules. The comprehensive ADMET profiling of compounds is provided in S-Table 2. Briefly, the compounds are accepted by Lipinski's rule of five (Lipinski, 2004). Per Lipinski's rule, compounds that adhere to this principle are more likely to possess favorable oral bioavailability, leading to increased gastrointestinal absorption and distribution.

Similarly, the compounds have zero alert for the pan-assay interference compounds (PAINS) (Whitty, 2011). The zero alerts for PAINS ensure that the investigated molecules will interact with a single specific biological target and might not cause any false positive results in a high throughput virtual screening process. The synthetic accessibility score CHEMBRIDGE-10000196 and CHEMBRIDGE-10000295 was observed less than 6, which mean that the compounds can be easily synthesized experimentally and can be used for biological activities validation. Additionally, the compounds were categorized to have less cytotoxicity and are non-mutagenic, which are essential parameters in drug discovery and design.
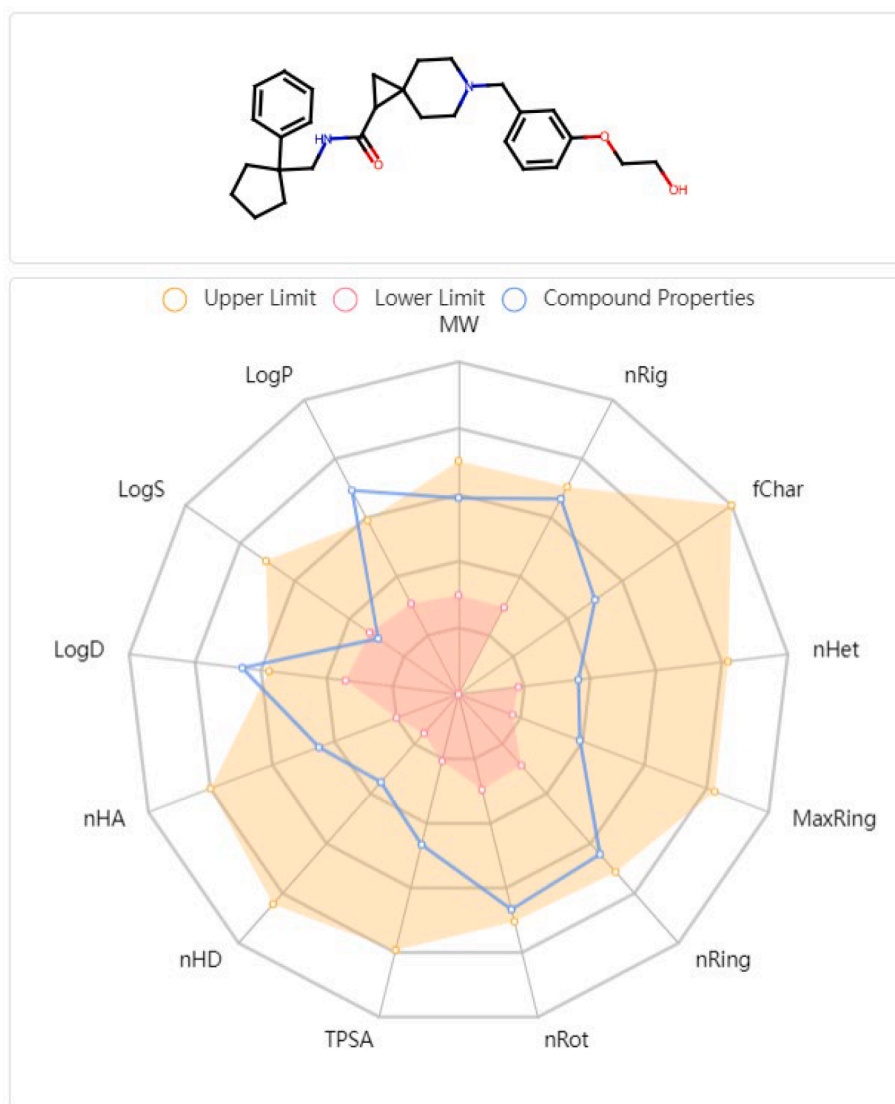
Fig. 7. ADMET profiling of CHEMBRIDGE-10000295. The yellow shadow and pink regions represent upper limits and lower limits, respectively while the blue line stands for compound properties. (For interpretation of the references to colour in this figure legend, the reader is referred to the web version of this article.)

4. Discussion

The burden of *H. pylori* infection on the developing countries' healthcare system is significant. This results in poor management of the infection and leads to a higher mortality rate (Hussein et al., 2021). The *H. pylori* burden is observed to be in high prevalence among children and adolescents (Liou et al., 2020). To effectively tackle the pathogen, appropriate screening combined with early identification can be helpful to avoid complications (Hutchings et al., 2019). From a treatment perspective, serious efforts are needed to look for new biological pathways and targets against the pathogen (Van Drie, 2007). Traditional techniques though quite successful in the past take a lot of time and often fail.

In contrast, computational techniques based on genomics and proteomic data can speed up novel target identification and subsequently new drug molecules (Siva Kumar et al., 2022). In particular, the implementation of artificial intelligence, machine learning and biophysics-based techniques proved to be highly useful in this regard (Bajorath et al., 2020). The CADD approaches have been successfully applied to identify promising inhibitors against the targeted enzyme. In one study, using different CADD techniques, a top compound "B5" was

identified as a promising inhibitor of the DNA excision repair protein ERCC-1 and DNA repair endonuclease XPF complex. The compound is also proven experimentally to show active biological potency (IC_{50} = 0.49 μM) (Gentile et al., 2020). In another work, FDA-approved drugs were found to show potent binding with the SARS-CoV-2 binding receptor, the angiotensin-converting enzyme-2 (Ahmad et al., 2021). In this work, the use of different applications and software based on machine learning, artificial intelligence and biophysics principles allowed us to predict three promising lead structures (CHEMBRIDGE-10000196, CHEMBRIDGE-10000295, and CHEMBRIDGE-1000095) against *H. pylori* XGHPRT enzyme. The compounds were proved to show stable binding to the enzyme active site and revealed robust chemical interaction patterns. Therefore, it is highly suggested to use the compounds in different enzyme-based assays to test the biological effectiveness of the drugs.

5. Concluding remarks

In this work, three compounds namely CHEMBRIDGE-10000196, CHEMBRIDGE-10000295, and CHEMBRIDGE-1000095 were identified as the best binders of *H. pylori* XGHPRT enzyme. These predictions were
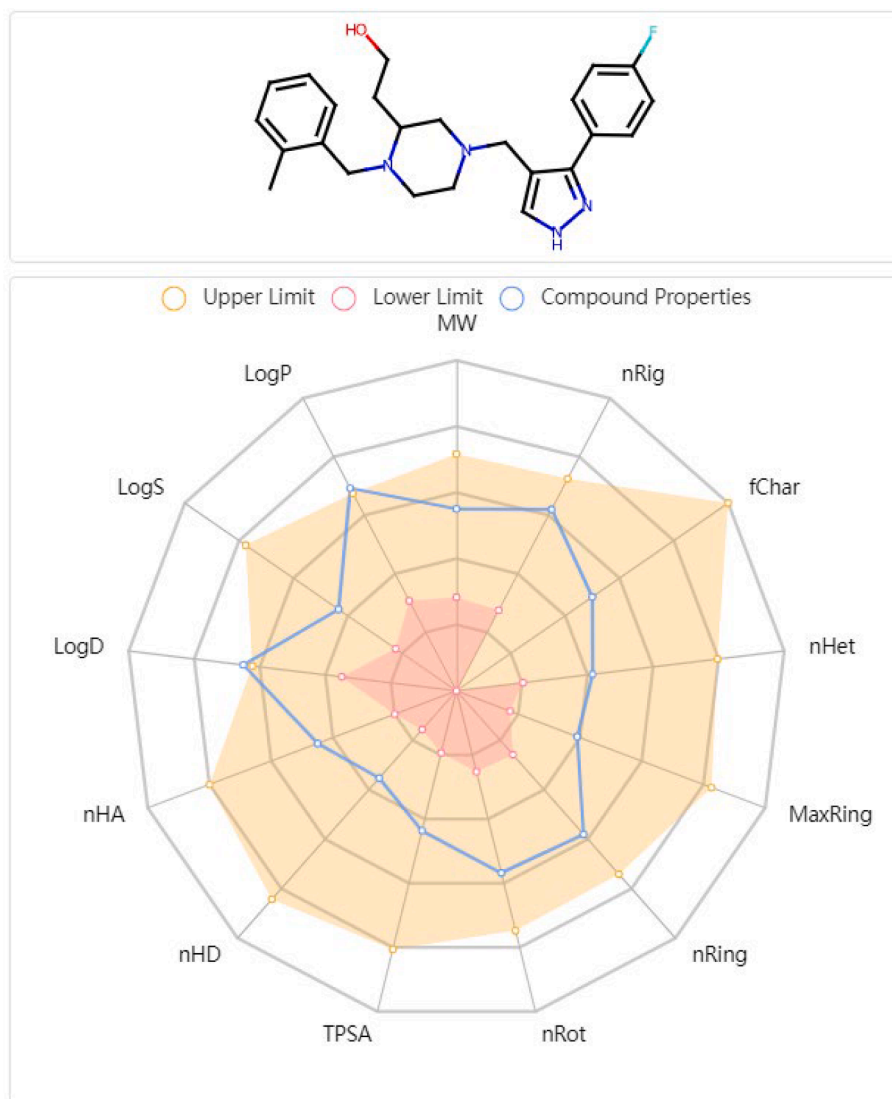
Fig. 8. ADMET profiling of CHEMBRIDGE-10000955. The yellow shadow and pink regions represent upper limits and lower limits, respectively while the blue line stands for compound properties. (For interpretation of the references to colour in this figure legend, the reader is referred to the web version of this article.)

made based on machine learning, artificial intelligence and biophysics-based principles. The compounds dock deep inside the pocket between the N-terminus and a long flexible loop. Multiple hydrogen bonding and van der Waals interactions were reported in compounds docking with the XGHPRT enzyme. The balance interactions of compounds with the enzyme demonstrate stable docked and dynamic behavior of complexes. Although the results of the present study display promising results, it is important to acknowledge that the lack of experimental testing is one of the main limitations of the work. Such studies could provide valuable insights into the biological characteristics of these molecules and their potential applications in relevant fields. Nevertheless, the study findings might be useful in speeding up drug discovery and optimization against XGHPRT in general and specifically against *H. pylori*.

CRediT authorship contribution statement

Alhumaidi B. Alabbas: Conceptualization, Funding acquisition, Data curation, Writing – original draft, Writing – review & editing, Visualization, Investigation, Validation, Formal analysis, Methodology, Supervision, Resources, Project administration and Software.

Declaration of competing interest

The authors declare that they have no known competing financial interests or personal relationships that could have appeared to influence the work reported in this paper.

Appendix A. Supplementary material

Supplementary data to this article can be found online at https://doi.org/10.1016/j.sjbs.2024.103960.

References

Ahmad, S., Raza, S., Uddin, R., Azam, S.S., 2017. Binding mode analysis, dynamic simulation and binding free energy calculations of the MurF ligase from Acinetobacter baumannii. J. Mol. Graph. Model. 77, 72–85. https://doi.org/10.1016/j.jmgm.2017.07.024.

Ahmad, S., Raza, S., Uddin, R., Azam, S.S., 2018. Comparative subtractive proteomics based ranking for antibiotic targets against the dirtiest superbug: Acinetobacter baumannii. J. Mol. Graph. Model. 82, 74–92. https://doi.org/10.1016/j.jmgm.2018.04.005.

Ahmad, S., Navid, A., Akhtar, A.S., Azam, S.S., Wadood, A., Pérez-Sánchez, H., 2019a. Subtractive genomics, molecular docking and molecular dynamics simulation revealed LpxC as a potential drug target against multi-drug resistant Klebsiella pneumoniae. Interdiscip. Sci. Comput. Life Sci. 11, 508–526.

Ahmad, S., Raza, S., Abro, A., Liedl, K.R., Azam, S.S., 2019b. Toward novel inhibitors against KdsB: a highly specific and selective broad-spectrum bacterial enzyme. J. Biomol. Struct. Dyn. 37, 1326–1345.

Ahmad, S., Waheed, Y., Abro, A., Abbasi, S.W., Ismail, S., 2021. Molecular screening of glycyrrhizin-based inhibitors against ACE2 host receptor of SARS-CoV-2. J. Mol. Model. 27, 206.

Alamri, M.A., Mirza, M.U., Adeel, M.M., Ashfaq, U.A., Tahir ul Qamar, M., Shahid, F., Ahmad, S., Alatawi, E.A., Albalawi, G.M., Allemailem, K.S., 2022. Structural elucidation of rift valley fever virus L protein towards the discovery of its potential inhibitors. Pharmaceuticals 15, 659.

Alamri, M.A., Tariq, M.H., Tahir ul Qamar, M., Alabbas, A.B., Alqahtani, S.M., Ahmad, S., 2023. Discovery of potential phytochemicals as inhibitors of TcdB, a major virulence factors of Clostridioides difficile. J. Biomol. Struct. Dyn. 1–9.

Altharawi, A., Ahmad, S., Alamri, M.A., ul Qamar, M.T., 2021. Structural insight into the binding pattern and interaction mechanism of chemotherapeutic agents with Sorcin by docking and molecular dynamic simulation. Colloids Surf. B Biointerfaces, 112098.

Andersen, H.C., 1983. Rattle: a "velocity" version of the shake algorithm for molecular dynamics calculations. J. Comput. Phys. 52, 24–34.

Australia, W., Robin, J., 2005. The 2005 Nobel Prize in physiology or medicine: Helicobacter pylori and its role in gastritis and peptic ulcer disease. Curr. Sci. 89.

Bajorath, J., Kearnes, S., Walters, W.P., Meanwell, N.A., Georg, G.I., Wang, S., 2020. Artificial intelligence in drug discovery: into the great wide open. J. Med. Chem.

Bergström, C.A.S., Larsson, P., 2018. Computational prediction of drug solubility in water-based systems: qualitative and quantitative approaches used in the current drug discovery and development setting. Int. J. Pharm. 540, 185–193.

Biovia, D., 2017. Discovery studio visualizer. San Diego, CA, USA.

Case, D.A., Cheatham III, T.E., Darden, T., Gohlke, H., Luo, R., Merz Jr, K.M., Onufriev, A., Simmerling, C., Wang, B., Woods, R.J., 2005. The Amber biomolecular simulation programs. J. Comput. Chem. 26, 1668–1688.

Coates, M.M., Kintu, A., Gupta, N., Wroe, E.B., Adler, A.J., Kwan, G.F., Park, P.H., Rajbhandari, R., Byrne, A.L., Casey, D.C., et al., 2020. Burden of non-communicable diseases from infectious causes in 2017: a modelling study. Lancet Glob. Heal. 8, e1489–e1498.

Dallakyan, S., Olson, A.J., 2015. Small-molecule library screening by docking with PyRx. In: Springer, pp. 243–250.

Du, X., Li, Y., Xia, Y.-L., Ai, S.-M., Liang, J., Sang, P., Ji, X.-L., Liu, S.-Q., 2016. Insights into protein–ligand interactions: mechanisms, models, and methods. Int. J. Mol. Sci. 17, 144.

El Bakri, Y., Lai, C.-H., Karthikeyan, S., Guo, L., Ahmad, S., Ben-Yahya, A., Mague, J.T., Essassi, E.M., 2021. Synthesis, crystal structure, Hirshfeld surface analysis and computational approach of new 2-methylbenzimidazo [1, 2-a] pyrimidin-4 (1H)-one. J. Mol. Struct. 1239, 130497.

Fatima, I., Ahmad, S., Alamri, M.A., Mirza, M.U., ul Qamar, M., Rehman, A., Shahid, F., Alatawi, E.A., Alkhayl, F.F.A., Al-Megrin, W.A., et al., 2022. Discovery of Rift Valley fever virus natural pan-inhibitors by targeting its multiple key proteins through computational approaches. Sci. Rep. 12, 9260.

Genheden, S., Kuhn, O., Mikulskis, P., Hoffmann, D., Ryde, U., 2012. The normal-mode entropy in the MM/GBSA method: effect of system truncation, buffer region, and dielectric constant. J. Chem. Inf. Model. 52, 2079–2088.

Gentile, F., Elmenoufy, A.H., Ciniero, G., Jay, D., Karimi-Busheri, F., Barakat, K.H., Weinfeld, M., West, F.G., Tuszynski, J.A., 2020. Computer-aided drug design of small molecule inhibitors of the ERCC1-XPF protein–protein interaction. Chem. Biol. Drug Des. 95, 460–471.

Halgren, T.A., 1996. Merck molecular force field. J. Comput. Chem. 17, 490–519. https://doi.org/10.1002/(SICI)1096-987X(199604)17:5/6<520::AID-JCC2>3.0.CO;2-W.

Hedstrom, L., 2009. IMP dehydrogenase: structure, mechanism, and inhibition. Chem. Rev. 109, 2903–2928.

Hussein, R.A., Al-Ouqaili, M.T.S., Majeed, Y.H., 2021. Detection of Helicobacter Pylori infection by invasive and non-invasive techniques in patients with gastrointestinal diseases from Iraq: a validation study. PLoS One 16, e0256393.

Hutchings, M., Truman, A., Wilkinson, B., 2019. Antibiotics: past, present and future. Curr. Opin. Microbiol. 51, 72–80. https://doi.org/10.1016/j.mib.2019.10.008.

Izaguirre, J.A., Catarello, D.P., Wozniak, J.M., Skeel, R.D., 2001. Langevin stabilization of molecular dynamics. J. Chem. Phys. 114, 2090–2098.

Jendele, L., Krivak, R., Skoda, P., Novotny, M., Hoksza, D., 2019. PrankWeb: a web server for ligand binding site prediction and visualization. Nucleic Acids Res. 47, W345–W349.

Jia, C.-Y., Li, J.-Y., Hao, G.-F., Yang, G.-F., 2019. A drug-likeness toolbox facilitates ADMET study in drug discovery. Drug Discov. Today.

Kaliappan, S., Bombay, I.I.T., 2018. UCSF Chimera-Overview.

Keough, D.T., Hockova, D., Holy, A., Naesens, L.M.J., Skinner-Adams, T.S., de Jersey, J., Guddat, L.W., 2009. Inhibition of hypoxanthine-guanine phosphoribosyltransferase by acyclic nucleoside phosphonates: a new class of antimalarial therapeutics. J. Med. Chem. 52, 4391–4399.

Keough, D.T., Hockova, D., Janeba, Z., Wang, T.-H., Naesens, L., Edstein, M.D., Chavchich, M., Guddat, L.W., 2015. Aza-acyclic nucleoside phosphonates containing a second phosphonate group as inhibitors of the human, Plasmodium falciparum and vivax 6-oxopurine phosphoribosyltransferases and their prodrugs as antimalarial agents. J. Med. Chem. 58, 827–846.

Keough, D.T., Rejman, D., Pohl, R., Zborn\\iková, E., Hocková, D., Croll, T., Edstein, M.D., Birrell, G.W., Chavchich, M., Naesens, L.M.J., et al., 2018. Design of Plasmodium vivax hypoxanthine-guanine phosphoribosyltransferase inhibitors as potential antimalarial therapeutics. ACS Chem. Biol. 13, 82–90.

Keough, D.T., Wun, S.J., Baszczynski, O., Eng, W.S., Spacek, P., Panjikar, S., Naesens, L., Pohl, R., Rejman, D., Hockova, D., et al., 2021. Helicobacter pylori xanthine–guanine–hypoxanthine phosphoribosyltransferase—a putative target for drug discovery against gastrointestinal tract infections. J. Med. Chem. 64, 5710–5729.

Kim, J., Wang, T.C., 2021. Helicobacter pylori and gastric cancer. Gastrointest. Endosc. Clin. 31, 451–465.

Laskowski, R.A., Jabłońska, J., Pravda, L., Vařeková, R.S., Thornton, J.M., 2018. PDBsum: structural summaries of PDB entries. Protein Sci. 27, 129–134.

Liou, J.-M., Malfertheiner, P., Lee, Y.-C., Sheu, B.-S., Sugano, K., Cheng, H.-C., Yeoh, K.-G., Hsu, P.-I., Goh, K.-L., Mahachai, V., et al., 2020. Screening and eradication of Helicobacter pylori for gastric cancer prevention: the Taipei global consensus. Gut 69, 2093–2112.

Lipinski, C.A., 2004. Lead- and drug-like compounds: the rule-of-five revolution. Drug Discov. Today Technol. 1, 337–341. https://doi.org/10.1016/j.ddtec.2004.11.007.

Lobanov, M.Y., Bogatyreva, N.S., Galzitskaya, O.V., 2008. Radius of gyration as an indicator of protein structure compactness. Mol. Biol. 42, 623–628.

Macalino, S.J.Y., Gosu, V., Hong, S., Choi, S., 2015. Role of computer-aided drug design in modern drug discovery. Arch. Pharm. Res. 38, 1686–1701.

Maier, J.A., Martinez, C., Kasavajhala, K., Wickstrom, L., Hauser, K.E., Simmerling, C., 2015. ff14SB: improving the accuracy of protein side chain and backbone parameters from ff99SB. J. Chem. Theory Comput. 11, 3696–3713.

Maiorov, V.N., Crippen, G.M., 1994. Significance of root-mean-square deviation in comparing three-dimensional structures of globular proteins.

Mezmale, L., Coelho, L.G., Bordin, D., Leja, M., 2020. Epidemiology of Helicobacter pylori. Helicobacter 25, e12734.

Miller, B.R., McGee, T.D., Swails, J.M., Homeyer, N., Gohlke, H., Roitberg, A.E., 2012. MMPBSA.py: an efficient program for end-state free energy calculations. J. Chem. Theory Comput. 8, 3314–3321. https://doi.org/10.1021/ct300418h.

Navid, A., Ahmad, S., Sajjad, R., Raza, S., Azam, S.S., 2021. Structure based in silico screening revealed a potent Acinetobacter baumannii Ftsz inhibitor from asinex antibacterial library. IEEE/ACM Trans. Comput. Biol. Bioinforma. 19, 3008–3018.

Pires, D.E.V., Blundell, T.L., Ascher, D.B., 2015. pkCSM: Predicting small-molecule pharmacokinetic and toxicity properties using graph-based signatures. J. Med. Chem. 58, 4066–4072. https://doi.org/10.1021/acs.jmedchem.5b00104.

Raza, S., Abbas, G., Azam, S.S., 2019. Screening pipeline for Flavivirus based inhibitors for Zika virus NS1. IEEE/ACM Trans. Comput. Biol. Bioinforma. 17, 1751–1761.

Roe, D.R., Cheatham III, T.E., 2013. PTRAJ and CPPTRAJ: software for processing and analysis of molecular dynamics trajectory data. J. Chem. Theory Comput. 9, 3084–3095.

Sangavai, C., Prathiviraj, R., Chellapandi, P., 2020. Functional prediction, characterization, and categorization of operome from Acetoanaerobium sticklandii DSM 519. Anaerobe 61, 102088.

Shaker, B., Ahmad, S., Lee, J., Jung, C., Na, D., 2021. In silico methods and tools for drug discovery. Comput. Biol. Med., 104851

Siva Kumar, B., Anuragh, S., Kammala, A.K., Ilango, K., 2022. Computer aided drug design approach to screen phytoconstituents of Adhatoda vasica as potential inhibitors of SARS-CoV-2 main protease enzyme. Life 12, 315.

Sprenger, K.G., Jaeger, V.W., Pfaendtner, J., 2015. The general AMBER force field (GAFF) can accurately predict thermodynamic and transport properties of many ionic liquids. J. Phys. Chem. B 119, 5882–5895.

Sussman, J.L., Lin, D., Jiang, J., Manning, N.O., Prilusky, J., Ritter, O., Abola, E.E., 1998. Protein Data Bank (PDB): database of three-dimensional structural information of biological macromolecules. Acta Crystallogr. D Biol. Crystallogr. 54, 1078–1084.

Sydow, D., Morger, A., Driller, M., Volkamer, A., 2019. TeachOpenCADD: a teaching platform for computer-aided drug design using open source packages and data. J. Cheminform. 11, 29.

Tacconelli, E., Carrara, E., Savoldi, A., Harbarth, S., Mendelson, M., Monnet, D.L., Pulcini, C., Kahlmeter, G., Kluytmans, J., Carmeli, Y., et al., 2018a. Discovery, research, and development of new antibiotics: the WHO priority list of antibiotic-resistant bacteria and tuberculosis. Lancet Infect. Dis. 18, 318–327.

Tacconelli, E., Carrara, E., Savoldi, A., Harbarth, S., Mendelson, M., Monnet, D.L., Pulcini, C., Kahlmeter, G., Kluytmans, J., Carmeli, Y., Ouellette, M., Outterson, K., Patel, J., Cavaleri, M., Cox, E.M., Houchens, C.R., Grayson, M.L., Hansen, P., Singh, N., Theuretzbacher, U., Magrini, N., Aboderin, A.O., Al-Abri, S.S., Awang Jalil, N., Benzonana, N., Bhattacharya, S., Brink, A.J., Burkert, F.R., Cars, O., Cornaglia, G., Dyar, O.J., Friedrich, A.W., Gales, A.C., Gandra, S., Giske, C.G., Goff, D.A., Goossens, H., Gottlieb, T., Guzman Blanco, M., Hryniewicz, W., Kattula, D., Jinks, T., Kanj, S.S., Kerr, L., Kieny, M.P., Kim, Y.S., Kozlov, R.S., Labarca, J., Laxminarayan, R., Leder, K., Leibovici, L., Levy-Hara, G., Littman, J., Malhotra-Kumar, S., Manchanda, V., Moja, L., Ndoye, B., Pan, A., Paterson, D.L., Paul, M., Qiu, H., Ramon-Pardo, P., Rodríguez-Baño, J., Sanguinetti, M., Sengupta, S., Sharland, M., Si-Mehand, M., Silver, L.L., Song, W., Steinbakk, M.,

Thomsen, J., Thwaites, G.E., van der Meer, J.W., Van Kinh, N., Vega, S., Villegas, M. V., Wechsler-Fördös, A., Wertheim, H.F.L., Wesangula, E., Woodford, N., Yilmaz, F. O., Zorzet, A., 2018b. Discovery, research, and development of new antibiotics: the WHO priority list of antibiotic-resistant bacteria and tuberculosis. Lancet Infect. Dis. 18 https://doi.org/10.1016/S1473-3099(17)30753-3.

Tahir ul Qamar, M., Ahmad, S., Fatima, I., Ahmad, F., Shahid, F., Naz, A., Abbasi, S.W., Khan, A., Mirza, M.U., Ashfaq, U.A., Chen, L.-L., 2021. Designing multi-epitope vaccine against Staphylococcus aureus by employing subtractive proteomics, reverse vaccinology and immuno-informatics approaches. Comput. Biol. Med. 132, 104389. 10.1016/j.compbiomed.2021.104389.

Talele, T.T., Khedkar, S.A., Rigby, A.C., 2010. Successful applications of computer aided drug discovery: moving drugs from concept to the clinic. Curr. Top. Med. Chem. 10, 127–141.

Turner, P.J., 2005. XMGRACE, Version 5.1. 19. Cent. Coast. Land-Margin Res. Oregon Grad. Inst. Sci. Technol. Beaverton, OR.

Van Drie, J.H., 2007. Computer-aided drug design: the next 20 years. J. Comput. Aided Mol. Des. 21, 591–601.

Wang, E., Sun, H., Wang, J., Wang, Z., Liu, H., Zhang, J.Z.H., Hou, T., 2019. End-point binding free energy calculation with MM/PBSA and MM/GBSA: strategies and applications in drug design. Chem. Rev. 119, 9478–9508.

Wang, J., Wang, W., Kollman, P.A., Case, D.A., 2001. Antechamber: an accessory software package for molecular mechanical calculations. J. Am. Chem. Soc. 222, U403.

Whitty, A., 2011. Growing PAINS in academic drug discovery. Future Med. Chem. 3, 797–801.

Woods, C.J., Malaisree, M., Michel, J., Long, B., McIntosh-Smith, S., Mulholland, A.J., 2014. Rapid decomposition and visualisation of protein-ligand binding free energies by residue and by water. Faraday Discuss. 169, 477–499. https://doi.org/10.1039/c3fd00125c.

Xiong, G., Wu, Z., Yi, J., Fu, L., Yang, Z., Hsieh, C., Yin, M., Zeng, X., Wu, C., Lu, A., et al., 2021. ADMETlab 2.0: an integrated online platform for accurate and comprehensive predictions of ADMET properties. Nucleic Acids Res. 49, W5–W14.